J Mater Sci: Mater Electron
DOI 10.1007/s10854-015-3436-y

Microstructural evolution of sputtered ZnO thin films with rapid thermal annealing

S. P. Ghosh[1] · K. C. Das[1] · N. Tripathy[1] · G. Bose[2] · D. H. Kim[4] · T. I. Lee[3] · J. M. Myoung[4] · J. P. Kar[1]

Received: 6 May 2015 / Accepted: 29 June 2015
© Springer Science+Business Media New York 2015

Abstract Zinc oxide thin films were deposited on silicon substrates by reactive RF magnetron sputtering technique. Post-deposition rapid thermal annealing of the sputtered thin films was carried out by varying temperatures, annealing duration and oxygen flow rate. The films, annealed at 1000 °C for 150 s in air ambient, have shown highest degree of crystallinity. The surface of the ZnO films, annealed for longer period, was greatly modulated with the evolution of porous surface. The films annealed in oxygen ambient have shown smoother morphology with the reduction in surface roughness. The characteristic absorption band of Zn–O became prominent due to the increase in Zn–O bond density during rapid thermal annealing process. A significant reduction of the deep level emission in the photoluminescence spectra was observed for annealed samples, whereas the near band edge ultraviolet emission was suppressed for the films annealed in oxygen ambient due to the oxygen adsorption at the film surface.

✉ J. P. Kar
karjp@nitrkl.ac.in

[1] Department of Physics and Astronomy, National Institute of Technology, Rourkela 769008, India

[2] Department of Electronics and Instrumentation Engineering, SOA University, Bhubaneswar 751030, India

[3] Department of Bio-Nanotechnology, Gachon University, Gyeonggi-do 461701, Republic of Korea

[4] Department of Materials Science and Engineering, Yonsei University, Seoul 120749, Republic of Korea

1 Introduction

Zinc oxide (ZnO) thin films have engrossed considerable interest now a days, due to its excellent material properties like piezoelectricity, large bandgap of 3.37 eV at room temperature and higher exciton binding energy (60 MeV), which is nearly two and half times greater than other direct bandgap semiconductors like gallium nitride (GaN) [1–3]. Therefore, ZnO is currently used as multifunctional electronic material having applications in numerous areas such as light emitting diodes, laser diodes, varistors, piezoelectric transducers, field-effect transistors, touch display panels, flat panel displays, photovoltaic solar cells, and gas sensors due to its high electrochemical stability, nontoxic nature, and ease of fabrication [4–6]. Basically, the synthesis of high quality ZnO thin film is mostly required for the enhancement in the performance of electronic devices. In current days, varieties of growth techniques are being implemented for deposition of thin films comprising of physical and chemical routes, such as pulsed laser deposition, thermal evaporation, chemical vapor deposition and magnetron sputtering [7–9]. Among these techniques, RF magnetron sputtering has several advantages such as its simplicity, low thermal budget, low-cost, nontoxic, and its ability to produce films of better quality with desired properties [10]. However, there is a chance of deterioration in the film quality due to the ionic bombardments or atomic intercollisions in the plasma during the sputtering, which generally gives rise to the formation of defects in the sputtered films. The electronic properties of the ZnO thin films are greatly influence by these defect densities [3, 11, 12]. Post-deposition heat treatments (annealing) are generally performed in order to annihilate the defects up to some extent [12]. Generally, annealing is broadly categorized into two types such as conventional furnace annealing

Published online: 23 July 2015

(CFA) and rapid thermal annealing (RTA). RTA has several advantages such as low thermal budget, short processing time and less chance of dopant distribution [13]. Although few researchers have attempted to conduct post-deposition RTA process of ZnO thin films [13–16], a systematic study on the effect of RTA temperature, annealing time and oxygen flow rate on the physical properties of sputtered ZnO films has not yet been completely explored. In this work, the influence of RTA temperature, annealing time and oxygen flow rate on the microstructural and optical properties of RF sputtered ZnO films are systematically investigated and correlated.

2 Experimental work

ZnO thin films were deposited onto n-type silicon [(100), 1–10 Ω cm] substrates using reactive radio frequency (RF) magnetron sputtering technique at a constant substrate temperature of 200 °C. A pure (99.99 %) metallic zinc target of 3 inch diameter was used as the zinc source. In order to generate the oxidation process of Zn, Ar/O_2 gas mixture was supplied to the sputtering chamber during film growth. The plasma was activated at an RF power of 150 W with a sputtering pressure of 4×10^{-3} mbar. Thereafter, post-deposition RTA of the sputtered films was carried out by varying temperature (from 400 to 1000 °C), annealing time (from 150 to 600 s) and oxygen flow rate (from 50 to 150 ml/min) using MTI (OTF 1200X) system.

After RTA treatment, structural property of ZnO films was investigated by X-ray diffraction (XRD, Rigaku/UltimaIV) with a CuKα ($\lambda = 0.154$ nm) radiation. The microstructures of the ZnO films were investigated using field-emission scanning electron microscope (FESEM: JEOL JSM-7001F). The surface topography of the samples was measured using atomic force microscopy (AFM, Asylum research system) operating in contact mode. The Fourier transform infrared (FTIR) spectra were recorded in the wavelength range of (400–2400 cm^{-1}) using Thermo scientific Nicolet 6700 system. In order to investigate the optical properties of ZnO film, photoluminescence (PL) spectral analysis has been carried out (Ramboss 500i) using He-Cd laser of wavelength 325 nm as the excitation source.

3 Results and discussion

Figure 1 shows the XRD pattern of ZnO films annealed at different RTA temperature ranging from 400 to 1000 °C in air ambient for 300 s. All the samples has shown c-axis orientation, where as a prominent (002) diffraction peak is observed for the sample annealed at 1000 °C. The gradual

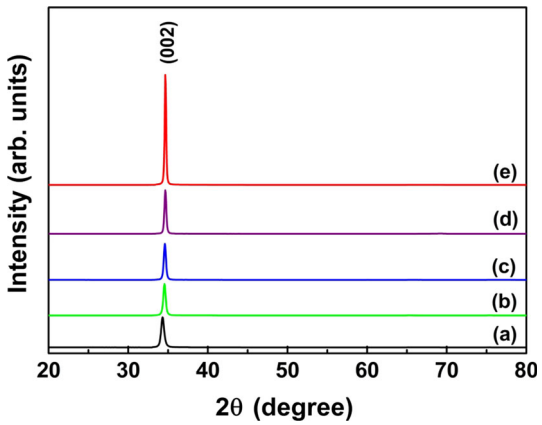

Fig. 1 X-ray diffraction patterns of ZnO thin films (*a*) as-deposited, and annealed at (*b*) 400 °C, (*c*) 600 °C, (*d*) 800 °C, (*e*) 1000 °C in air ambient for 300 s

increase in peak intensity signifies a progressive improvement in the crystallinity along c-axis. Nonstoichiometric ZnO thin films are generally formed due to the presence of zinc interstitials or oxygen vacancies, which are responsible for the n-type conductivity in ZnO [17, 18]. During annealing, the atoms migrate to the favorable positions after receiving adequate amount of thermal energy in order to annihilate the defects and restructuring of the films take place along (002) orientation. The growth along c-axis is preferred due to its smallest surface free energy in this particular orientation [19]. A shift in the (002) peak position towards higher diffraction angle attributes the stress relaxation due to the recrystallization and reduction of lattice imperfections of the annealed films in comparison to the as-deposited one [20].

Figure 2 shows the FESEM images of ZnO thin film annealed at different RTA temperatures for 300 s in air ambient. Figure 2a depicts the granular surface morphology of as-deposited sample. The surface morphology is significantly modulated due to the evolution of bigger grains for the annealing temperature of 1000 °C. In addition, structural modification is also observed with the appearance of small textures on the coalesced region. Figure 3 shows the evolution of surface roughness with the variation in the annealing temperature. A marginal increase in the roughness with the annealing temperature up to 800 °C is observed. The film, annealed at 1000 °C, has shown higher surface roughness, which may be due to the evolution of larger grains as revealed by our SEM studies. The enhancement of the grain size at higher annealing temperature may be due to the relocation of grain boundaries by coalescence of smaller grains. This motion of grain boundary is due to atomic diffusion in grains by receiving adequate amount of activation energy [21].

Figure 4 shows the XRD patterns of the ZnO thin films annealed at 1000 °C for a duration ranging from 150 to

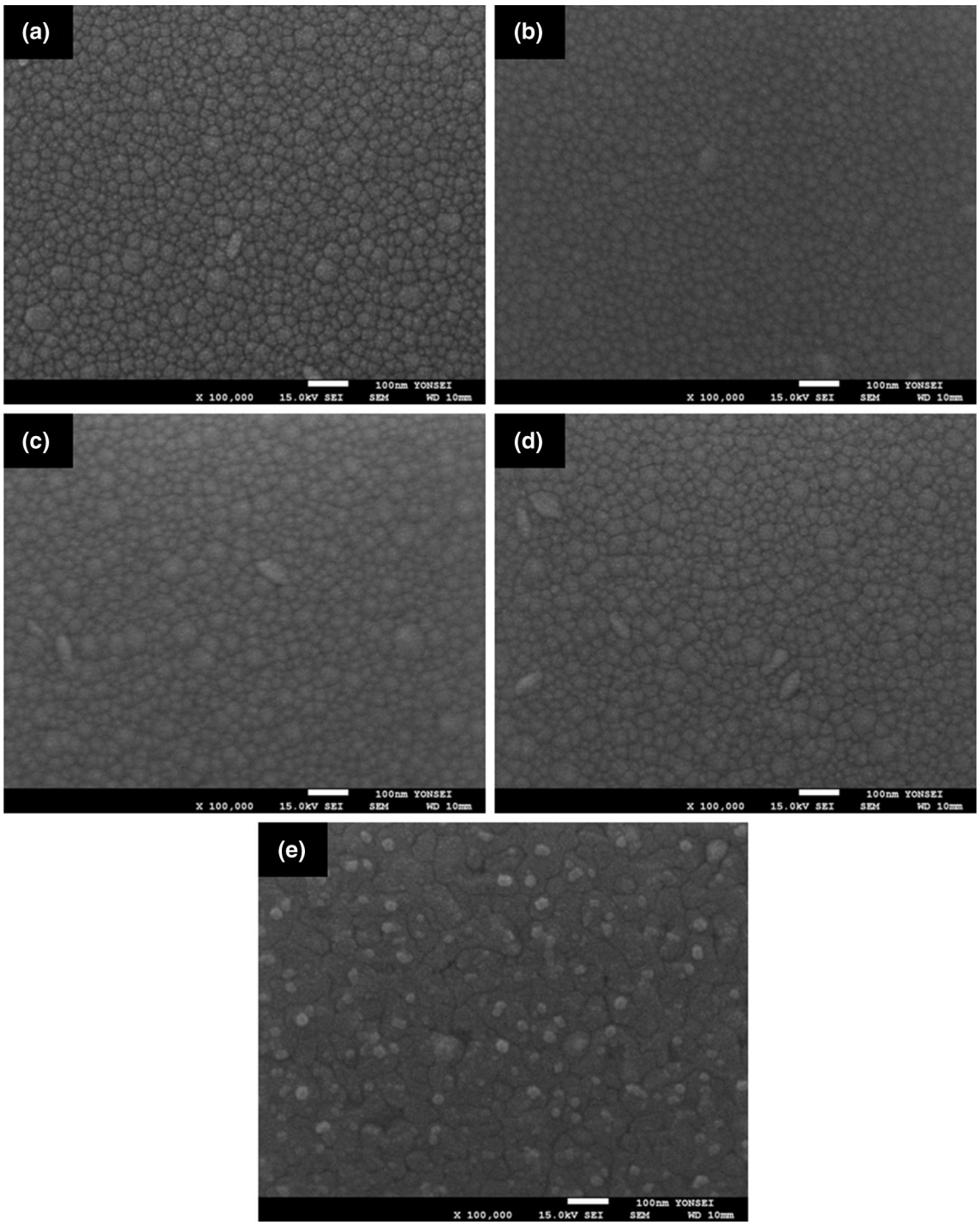

Fig. 2 FESEM images of ZnO thin films **a** as-deposited, and annealed at **b** 400 °C, **c** 600 °C, **d** 800 °C, and **e** 1000 °C in air ambient for 300 s. The *scale bar* represents 100 nm

600 s in air ambient. All the samples exhibit a prominent (002) diffraction peak, which corresponds to the preferential orientation of the annealed films along c-axis. However, this peak intensity is deteriorated with annealing time, which may be due to the structural modification in the annealed films. Figure 5 shows the FESEM images of ZnO thin film annealed at 1000 °C in air ambient by varying process duration. It has been observed that the secondary grain growth became prominent with increase in annealing duration. For annealing time of 150 s (Fig. 2e), newly generated smaller grains appeared on the coalesced bigger grain. This evolution of microstructures on the coalesced

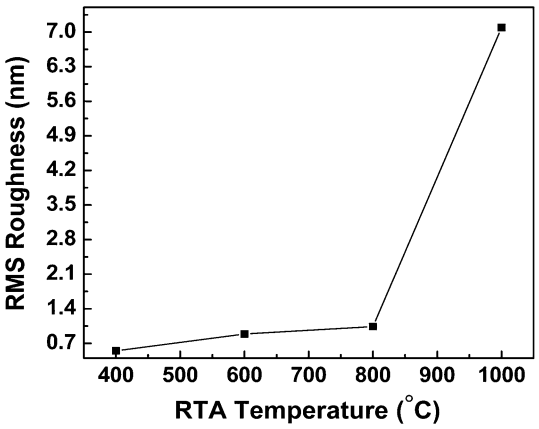

Fig. 3 Variation of RMS roughness of ZnO thin films annealed at various temperatures for 300 s in air ambient

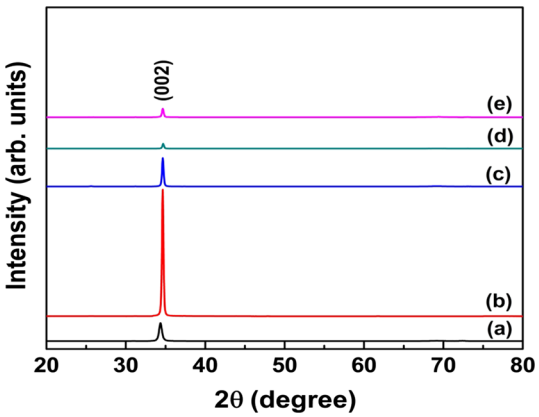

Fig. 4 X-ray diffraction patterns of ZnO thin films (*a*) as-deposited, and annealed at 1000 °C in air ambient for (*b*) 150 s, (*c*) 300 s, (*d*) 450 s, (*e*) 600 s

area became prominent with the increase in annealing time and as a result rough and porous surface is obtained. Longer annealing period provides sufficient time and thermal energy to the ZnO microstructures for subsequent growth. This kind of restructuring of the grains may lead to the formation of ZnO nanostructures, which is the scope of future research. Similar type of microstructural modulation has also been observed by Alvarado et al. [22]. The RMS roughness of the annealed films with various processing time is plotted in Fig. 6, where the roughness of the ZnO films is found to be increased with annealing time. The FESEM and AFM analysis are well agreed with the XRD results.

Figure 7 shows the XRD patterns of ZnO thin films annealed at 1000 °C for 150 s under different oxygen flow rate ranging from 50 to 150 ml/min. XRD plot of all the ZnO films exhibits a prominent (002) peak. The films, annealed at 150 ml/min, show higher degree of orientation in comparison to the flow rate of 50 ml/min. However, the films, annealed in air ambient, show better crystallinity. Figure 8 depicts the FESEM images of the ZnO films annealed at 1000 °C for 150 s under various oxygen flow rate. Larger grains are formed due to the Ostwald ripening, where larger crystallites were grown by consuming the smaller adjacent crystallites during annealing in oxygen ambient. Figure 9 shows the RMS roughness of the ZnO films with various oxygen flow rate during RTA process. The roughness of the film is found to be lowest for higher rate of oxygen flow due to the nonappearance of additional microstructures on its surface.

Figure 10 shows the Fourier transform infrared (FTIR) transmission spectra of ZnO thin films annealed at 1000 °C for 150 s with various annealing ambient. A broad band centered around 485 cm^{-1} is attributed to characteristic absorption band of Zn–O stretching mode [23–25]. As a result of annealing, the band becomes prominent, indicating an increase in Zn–O bond density. This increase in Zn–O bond network may be due to the diffusion of oxygen into the film during RTA process, which greatly depends on the annealing temperature and its ambient. In polycrystalline films, grain boundaries may act as channels for rapid incorporation of oxygen inside the film, which in fact enhances the microscopic rearrangement of Zn–O bond network through oxidation of Zn atoms. This band became prominent as a result of annealing, which could be associated with the improvement in the ZnO crystallinity. One more additional band centered at 1110 cm^{-1} corresponds to the Si–O stretching bond. [25]. Figure 11 shows PL spectra of ZnO/Si films annealed at 1000 °C for 150 s with various annealing ambient. A sharp UV emission peak has been observed for all the samples, which corresponds to the near band edge emission. This UV peak intensity became prominent for the films annealed in air ambient, which is attributed to the formation of stoichiometric ZnO films with the improvement in the crystallinity. In addition, annealed samples show a marginal blue shift at the near band edge emission, which attributes to the enhancement in the bandgap. The reduction in the bandgap may be due to the overlapping of the defect band and conduction band in the unannealed film. The appearance of the defect bands, in the visible region, are due to the existence of Zn interstitials in the unannealed sample, which in fact gives rise to the formation of shallow donors state [26]. RTA at high temperature suppressed these defect levels in order to enhance the bandgap and stoichiometry of ZnO films. However, the suppression of UV emission peak (Fig. 11b) may be due to the excess adsorption oxygen molecules at the surface as well as in the grain boundaries of the ZnO films during RTA process in oxygen ambient. This adsorbed oxygen gives rise to the accumulation of electrons from the oxygen vacancies on the surface of the ZnO film. A built-in electric field is formed on the surface of ZnO

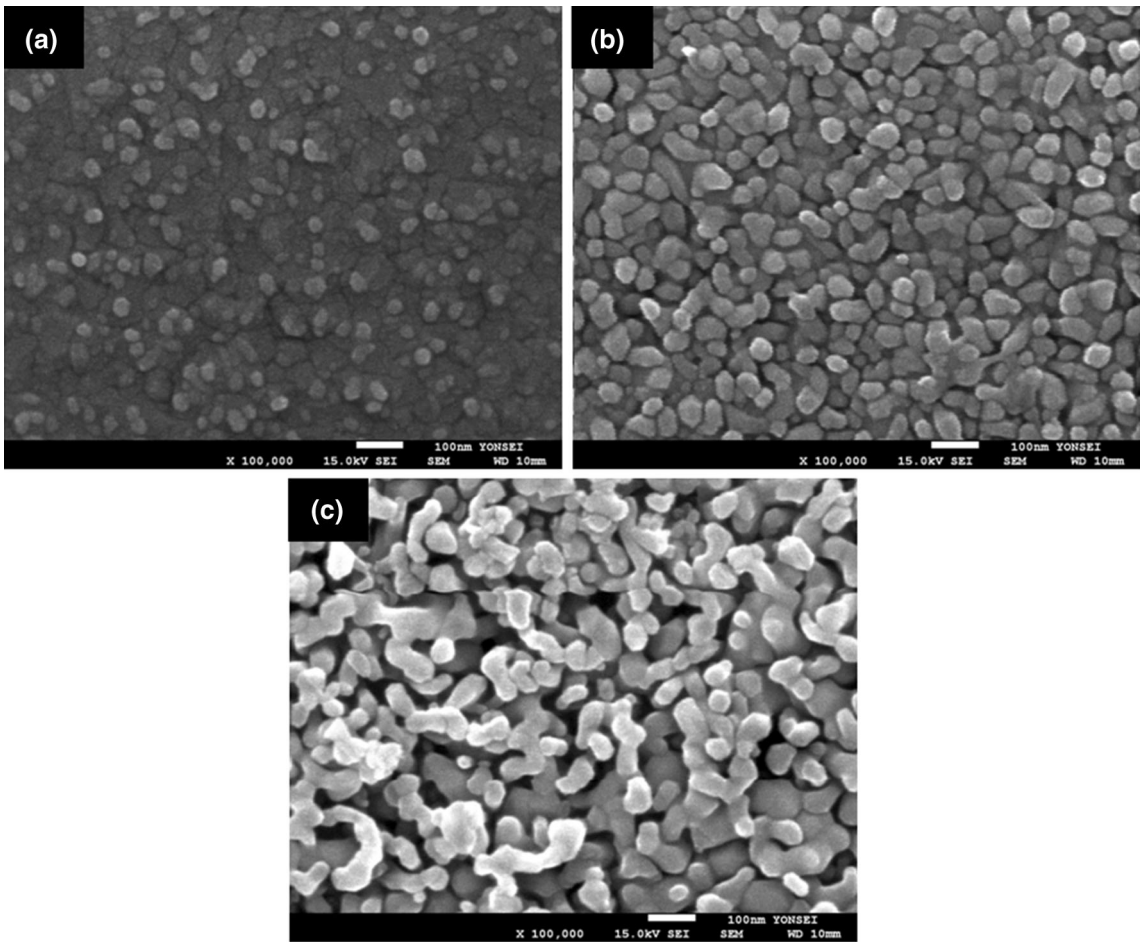

Fig. 5 FESEM images of ZnO thin films annealed at 1000 °C in air ambient for **a** 150 s, **b** 450 s, and **c** 600 s. The *scale bar* represents 100 nm

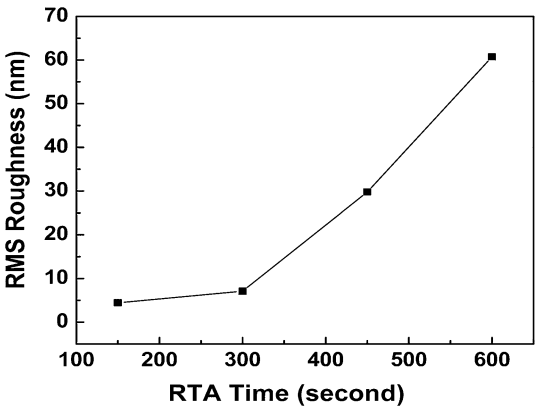

Fig. 6 Variation of RMS roughness of ZnO thin films annealed at 1000 °C in air ambient for various RTA duration

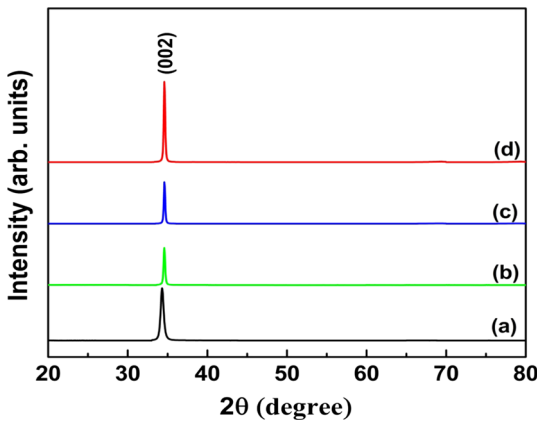

Fig. 7 X-ray diffraction patterns of ZnO thin films (*a*) as-deposited, and annealed at 1000 °C for 150 s with oxygen flow rate of (*b*) 50 ml/min, (*c*) 100 ml/min, and (*d*) 150 ml/min

film due to the presence of the negatively charged oxygen species and the electrons depleted from the underneath the surface of the ZnO film [27, 28]. Most of the photogenerated holes are driven towards the surface, whereas the photogenerated electrons are swept into the bulk of the ZnO film due to the presence of the depletion region. Therefore, the suppression in the UV emission peak is observed due to the significant reduction in the recombination probability of the photogenerated electrons and

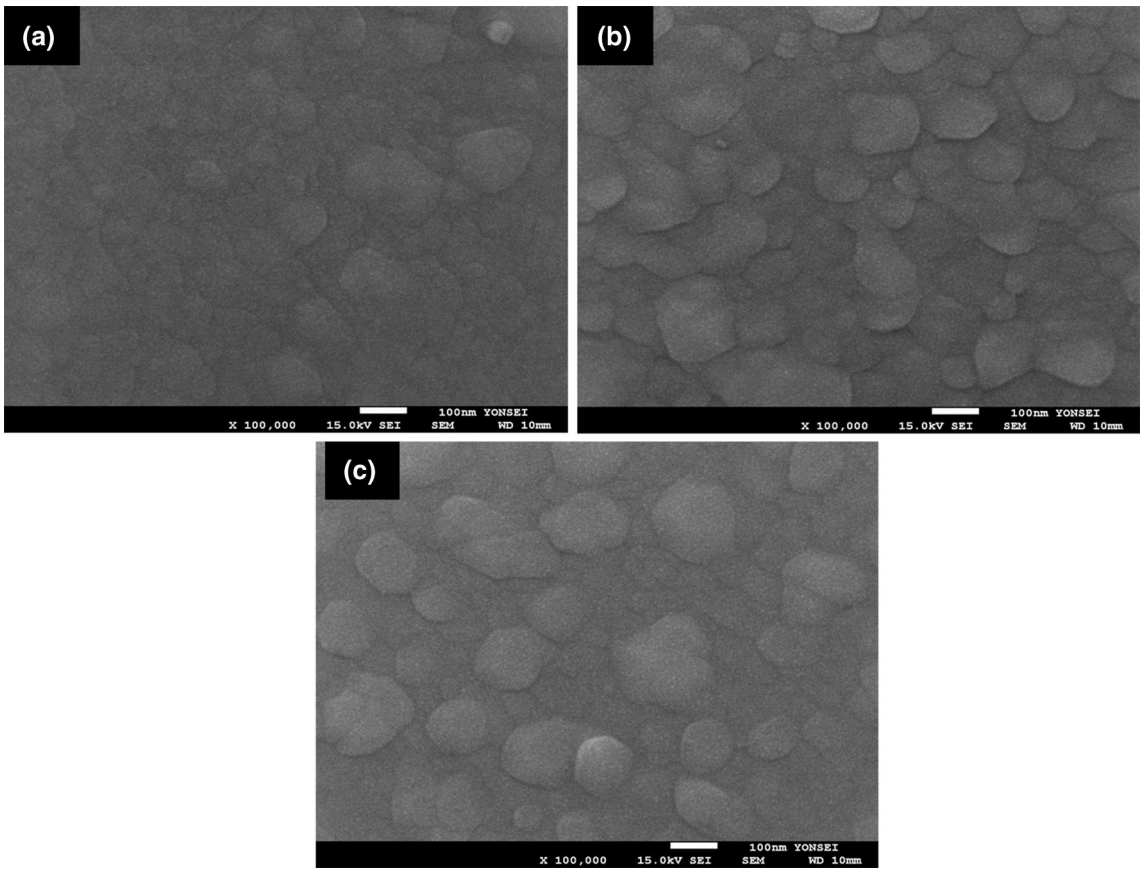

Fig. 8 FESEM images of ZnO thin films annealed at 1000 °C for 150 s with oxygen flow rate of **a** 50 ml/min, **b** 100 ml/min, and **c** 150 ml/min. The *scale bar* represents 100 nm

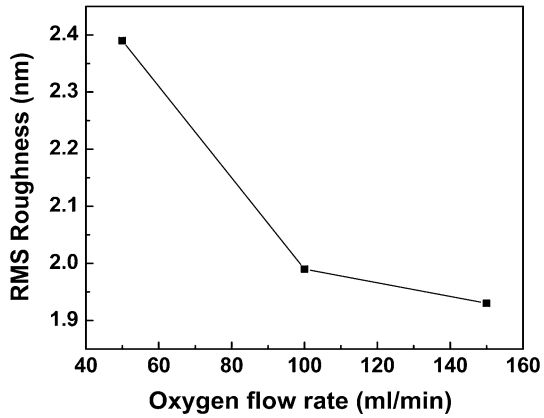

Fig. 9 Variation of RMS roughness of ZnO thin films annealed at 1000 °C for 150 s with various oxygen flow rate

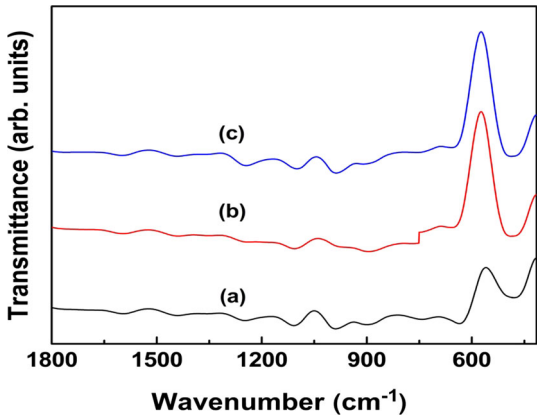

Fig. 10 FTIR transmittance spectra of ZnO thin films (*a*) as-deposited, and annealed at 1000 °C for 150 s (*b*) in air ambient, (*c*) with O_2 flow rate of 150 ml/min

holes for the films annealed at oxygen ambient. On the other hand, a broad deep level emission is observed for the as-deposited films in the visible range and its intensity remarkably reduced after high temperature RTA treatment. The suppression of this broad emission peak may be due to the reduction of the defects such as Zn interstitials, Zn vacancies, oxygen interstitials, oxygen vacancies and other impurities during RTA [29].

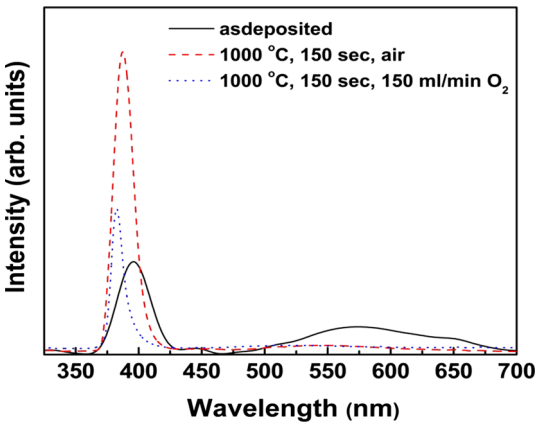

Fig. 11 Photoluminescence spectra of ZnO thin films with various annealing parameters

4 Conclusion

RF sputtered ZnO thin films were subjected to rapid thermal annealing with varying annealing parameters such as temperature, annealing duration and ambient. Relatively high c-axis (002) oriented films were obtained at 1000 °C in air ambient for an annealing duration of 150 s. The surface of the films, annealed for 600 s, became rough due to the evolution porous microstructures, whereas the films annealed in oxygen ambient has shown smoother surface morphology. The characteristic absorption band of Zn–O became prominent due to the increase in Zn–O bond density by the oxidation of unbounded zinc atoms during the RTA process. A significant reduction of the deep level emission in the photoluminescence spectra was observed for annealed samples, whereas the near band edge UV emission was suppressed for the films annealed in oxygen ambient due to the oxygen adsorption at the film surface.

Acknowledgments This work was supported by the Department of Science and Technology (DST), India sponsored Indo-Korea Project (INT/Korea/P-16/2013) and partly supported by DST Science and Engineering Research Board (SERB) Project (SR/FTP/PS-099/2012) under Fast Track Scheme for Young Scientist. This research was also supported by the International Research and Development Program of the National Research Foundation of Korea (NRF) funded by the Ministry of Science, ICT and Future Planning (Grant Number: 2012K1A3A1A19038371).

References

1. B.C. Mohanty, B.K. Kim, D.H. Yeon, Y.H. Jo, I.J. Choi, S.M. Lee, Y.S. Cho, J. Electrochem. Soc. **159**, H96–H101 (2012)
2. C. Wang, D. Xu, X. Xiao, J. Mater. Sci. **42**, 9795–9800 (2007)
3. U. Ozgur, Y.I. Alivov, C. Liu, A. Teke, M.A. Reshchikov, S. Dogan, V. Avrutin, S.J. Cho, H. Morkoc, J. Appl. Phys. **98**, 041301 (2005)
4. A. Radzimska, T. Jesionowski, Materials **7**, 2833–2881 (2014)
5. J. Mou, W. Zhang, J. Fan, H. Deng, W. Chen, J. Alloys Compd. **509**, 961–965 (2011)
6. J. Loureiro, S. Filonovich, N. Neves, R. Barros, S. Reparaz, L. Divay, T. Mateus, C. Torres, R. Martins, R. Santos, I. Ferreira, J. Mater. Chem. A **2**, 6649 (2014)
7. C.W. Hsu, T. Cheng, W. Huang, J. Wu, C. Cheng, K. Cheng, S. Huang, Thin Solid Films **518**(8), 1953–1957 (2010)
8. W. Mtangi, F.D. Auret, J. Rensburg, P.J. Coelho, S.M. Legodi, M.J. Nel, J.M. Meyer, A. Chawanda, J. Appl. Phys. **110**(9), 094504 (2011)
9. C. Periasamy, R. Prakash, P. Chakrabarti, J. Mater. Sci. Mater. Electron. **5**, 9912 (2009)
10. J.P. Kar, S. Kim, B. Shin, J.M. Myoung, Solid State Electron. **54**(11), 1447–1450 (2010)
11. K.C. Sekhar, S. Levichev, K. Kamakshi, S. Doyle, A. Chahboun, M.J.M. Gomes, Mater. Lett. **98**, 149–152 (2013)
12. G.P. Daniel, V.B. Justinvictor, P.B. Nair, K. Joy, P. Koshy, P.V. Thomas, Phys. B **405**, 1782–1786 (2010)
13. J. Li, J.H. Huang, Y. Zhang, Y. Yang, W. Song, X.M. Li, J. Electroceram. **26**, 84–89 (2011)
14. Y. Lee, S. Hu, W. Water, Y.S. Huang, M.D. Yang, J. Shen, K.K. Tiong, C. Huang, Solid State Commun. **143**, 250–254 (2007)
15. N.A. Suvorova, I.O. Usov, L. Stan, R.F. Paula, A.M. Dattelbaum, Q.X. Jia, A.A. Suvorova, Appl. Phys. Lett. **92**, 141911 (2008)
16. W. Cheong, M. Ryu, J. Shin, S. Park, C. Hwang, Thin Solid Films **516**, 8159–8164 (2008)
17. A.K. Srivastava, J. Kumar, Sci. Technol. Adv. Mater. **14**, 065002 (2013)
18. A. Janotti, C.G. Van de Walle, Rep. Prog. Phys. **72**, 126501 (2009)
19. P.T. Hsieh, Y.C. Chen, C.M. Wang, Y.Z. Tsai, C.C. Hu, Appl. Phys. A Mater. Sci. Process. **84**, 345–349 (2006)
20. G. Anil Kumar, M.V.R. Reddy, K.N. Reddy, J. Phys. Conf. Ser. **365**, 012031 (2012)
21. Z.W. Liu, W.J. Fu, M. Liu, J.F. Gu, C.Y. Ma, Q.Y. Zhang, Surf. Coat. Technol. **202**, 5410–5415 (2008)
22. J.A. Alvarado, A. Maldonado, H. Juarez, M. Pacio, R. Perez, Beilstein, J. Nanotechnol. **6**, 971–975 (2015)
23. S.Y. Hu, Y.C. Lee, J.W. Lee, J.C. Huang, J.L. Shen, W. Water, Appl. Surf. Sci. **254**, 1578–1582 (2008)
24. Y.C. Lee, S.Y. Hu, W. Water, K. Tiong, Z.C. Feng, T. Chen, J.C. Huang, J.W. Lee, C. Huang, J.L. Shen, M.H. Cheng, J. Lumin. **129**, 148–152 (2009)
25. K. Vijayalakshmi, K. Karthick, D. Gopalakrishna, Ceram. Int. **39**, 4749–4756 (2013)
26. A. Wang, T. Chen, S. Lu, Z. Wu, Y. Li, H. Chen, Y. Wang, Nanoscale Res. Lett. **10**, 75 (2015)
27. X. Yan, M. Yang, J. Lu, Y. De-Ren, Chin. Phys. Lett. **29**, 037301 (2011)
28. D. Wang, N. Reynolds, Int. Sch. Res. Netw. **6**, 950354 (2012)
29. H. Song, J. Kim, E. Kim, J. Korean Phys. Soc. **53**, 258–261 (2008)